



# In situ preparation of silver nanoparticle embedded composite nanofibrous membrane: a multi-layered biocidal air filter

Gobi Nallathambi<sup>1</sup> · Berly Robert<sup>1</sup>

Received: 6 May 2022 / Revised: 15 October 2022 / Accepted: 4 November 2022 /  
Published online: 11 November 2022

© The Author(s), under exclusive licence to Springer-Verlag GmbH Germany, part of Springer Nature 2022

## Abstract

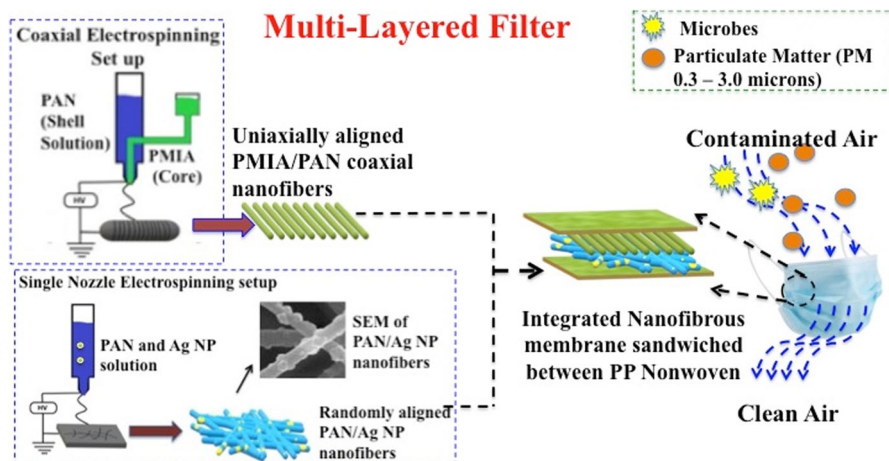
Deteriorating air quality has increased the need for designing composite integrated nanofibrous membranes, which are suitable for facemask technology providing efficient solution against microbial propagation and particulate matter. Through this research work, an aramid-based multilayered membrane is developed which provides significantly increased mechanical stability when compared to easily collapsing nanofibrous structures usually considered for air filtration applications. The developed filter is tested for its bacterial filtration efficiency through an Andersen sampler using *Staphylococcus aureus* as the challenge aerosol with mean particle size of  $3.0 \pm 0.3 \mu\text{m}$ . The Particulate Matter (with diameters ranging from 0.3 to 10  $\mu\text{m}$ ) filtration efficiency and Bacterial filtration efficiency of 99.41% and 99.51% was achieved, respectively, indicating its potential for applications ranging from facemasks (mainly for protection against airborne microorganisms) to industrial-scale air filters. Our study indicated that the combination of silver nanoparticles incorporated polyacrylonitrile nanofibers integrated with a layer of aramid based coaxial nanofibers offer a new strategy to construct advanced multifunctional membrane which could not only perform well as an antimicrobial filter but also remove particulate matter in air effectively.

---

✉ Berly Robert  
berlyrobert87@gmail.com

<sup>1</sup> Department of Textile Technology, Anna University, Chennai 600 025, India

## Graphical abstract



## Introduction

Polymer nanofibers with nanoparticles incorporated within have become an important class of nanomaterial. The widely used commercial micro-sized fibrous filters (e.g., spun-bond and melt blown nonwoven fabrics) suffer from various application drawbacks (mainly their incapability to capture particles with aerodynamic diameter  $< 2.5 \mu\text{m}$ ) [1]. Benefitting from smaller pore size, decrease in fiber diameter and large surface-to-volume ratio; electrospun nanofibrous membrane (NFM) has already gained significant importance in air filtration applications [2–5]. When these polymeric NFMs are tailored with various antibacterial agents they display enhanced antibacterial activity and the microbial filtration efficiencies are greater than 99%. They can be used as biocidal filter membrane to capture not only the particulate matter (PM) but also for capturing microbial contaminants [6–8]. When compared to liquid dip process, where the filters are submerged in an antibacterial liquid that result in pore blockage and an increase in pressure drop, these NFM integrate the antibacterial agents into each nanofiber without clogging the pores [9, 10].

Considering various advantages of electrospun polymeric NFMs, several studies exist with regard to usage of organic solvents to reduce metallic salts. At the same time organic solvents can be considered to effectively dissolve polymer. Ethanol has been the most popular solvent for synthesis of metal nanoparticles [11, 12]. Another interesting solvent that has proven to act as powerful reducing agent of silver (Ag) and gold nanoparticle synthesis is *N,N*-dimethylacetamide (DMAc) and *N,N*-dimethylformamide (DMF) [13, 14]. Moreover, DMF has been considered as one of the usual organic compound used as a solvent for electrospinning various polymeric components. In other words, DMF plays a dual role; as a solvent for various polymers and a powerful reducing agent. Consequently, polyacrylonitrile (PAN:

an easy to electrospin polymer) or polyvinylidene fluoride (PVDF) have been widely considered to develop composite NFM for aerosol and bacterial filtration [15, 16].

Apart from filtration efficiency and pressure drop of an air filter membrane, the tensile strength is a major factor that cannot be overlooked. The weak mechanical property and easily collapsing cavity structure of NFM can be addressed by using high performance polymers like polysulfone or polyurethane or meta-aramids [17–19]. Some polymers are not suitable to be used as materials for air filter medium. Nanofibers developed using polystyrene (PS) are brittle and have weak tensile properties. Similarly, nanofibers developed using Polyethylene oxide (PEO) and polyvinyl alcohol (PVA) produce water-soluble membranes [20]. PAN has been the most widely considered polymer to develop NFM for air filtration applications [21, 22]. They have low stiffness and very weak tensile properties. Hence, the developed PAN-based membrane will exhibit easily collapsing cavity structure indicating problem in practical application. For this purpose, in this work, PAN and Ag based NFM is integrated with a layer of uniaxially aligned meta-aramid based coaxial NFM, which would help in maintaining the essential mechanical properties of developed filter media.

Meta-aramids like poly(m-phenylene isophthalamide) (PMIA) also known commercially as Nomex are high performance polymers that can be considered to develop NFM which would exhibit outstanding mechanical properties [23, 24]. However, electrospinning PMIA at a relative humidity greater than 50% results in formation of nanofibers that get collected on a collector in bundles. Such membranes when used as an air filter medium will exhibit poor filtration efficiency. As a remediation, the property of PMIA can be enhanced by coaxial electrospinning, where an easily spinnable polymer can be considered as the sheath layer and a hard-to-spin polymer like PMIA as the core [25].

In this work, in situ Synthesis of Silver Nanoparticles (Ag NP) in PAN nanofiber is carried out and the resulting finest PAN/Ag NPs-based antibacterial NFM is integrated with PMIA/PAN-based uniaxially aligned NFM to develop a multilayered filter with stable cavity structure for application in air filtration of particulate and microbial contaminants.

## Materials and methods

The PMIA (Nomex 450) was procured from Arvind Limited, Gujarat, India. PAN (MW 150,000 g/mol) (CAS No: 25014-41-9) was obtained from Sigma-Aldrich, *N,N*-dimethylacetamide (DMAc) extra pure 99% (CAS No. 127-19-5), *N,N*-dimethylformamide (DMF) extra pure 99% (CAS No. 68-12-2), lithium chloride (LiCl) Anhydrous extra pure AR 99% (CAS No. 7447-41-8), Sodium Chloride (NaCl) extra pure AR 99.9% (CAS No. 7647-14-5), Nutrient broth (Product code: 55427), nutrient agar (Product code: 63971) and silver nitrate (AgNO<sub>3</sub>) extra pure 99.5% (CAS No. 7761-88-8) were all obtained from SRL chemicals, India. *Bacillus subtilis* (*B. subtilis*) and *Escherichia coli* (*E. coli*) were obtained from Microbial Type Culture Collection, India. All chemicals were of analytical grade and used as received without further purification.

**Fig. 1** Formation of silver nanoparticles (Ag NPs); **a** PAN in DMF solution; **b** PAN and  $\text{AgNO}_3$  solution; **c–e** PAN and  $\text{AgNO}_3$  solution after 15 min, 25 and 35 min heat treatment, respectively

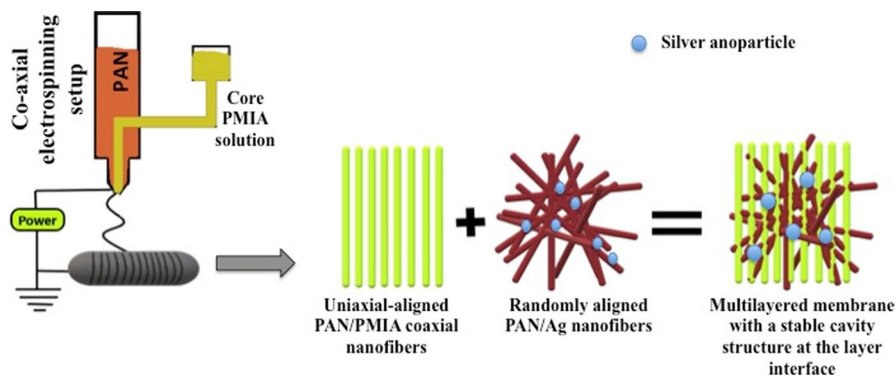
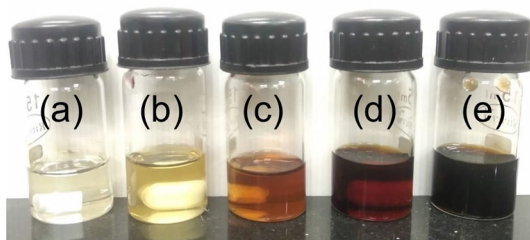


**Fig. 2** Preparation process of integrated nanofibrous composite membrane

### In situ synthesis of Ag nanoparticles in PAN nanofibers

PAN/Ag NP-based nanofibers were prepared by dissolving different percentages of  $\text{AgNO}_3$  (3, 5, 7, 9, 11, 13, 15, 17 and 19 wt.% based on weight of PAN) with PAN (8 wt.%) in 5 mL DMF, to form nine homogenous PAN/ $\text{AgNO}_3$  solutions. The solutions were light-protected and stirred at around 60 °C for 2 h till a reddish-brown color confirming the reduction in silver ions, and subsequent formation of silver atoms as shown in Fig. 1 was noted. The PAN/Ag NP electrospun NFM with different  $\text{AgNO}_3$  wt.% as 3, 5, 7, 9, 11, 13, 15, 17 and 19 were named as S3, S5, S7, S9, S11, S13, S15, S17 and S19, respectively.

### Preparation of multilayered electrospun nanofibrous membrane

To electrospin PAN (as shell)/PMIA (as core) based coaxial nanofibers, a homogeneous PMIA solution (8 wt.% concentration) was prepared by dissolving PMIA fibers in ionic liquid DMAc/LiCl (1 wt.% LiCl). The solution was stirred at 80–100 °C for 12 h. Simultaneously, in a separate vial 8 wt.% PAN solution was prepared by dissolving PAN in DMF. This PAN solution was stirred for around 3 h at room temperature.

As shown in Fig. 2, a coaxial electrospinning set-up was used to eject PMIA and PAN polymeric solution through a co-axial capillary. The nanofibers produced through coaxial-electrospinning is an innovative extension of traditional electrospinning approach. The main deviation is at the spinneret, which comprises of a blunt-type stainless steel needle (a very small capillary) inserted concentrically inside a bigger capillary. The inner capillary (with 0.5 mm inner diameter) and outer capillary (with 1.0 mm diameter) tubes are connected to respective syringe pumps.

The nozzle tip-to-collector distance was 10 cm, and flow rates of inner PMIA and outer PAN precursor solutions were 0.10 and 0.20 mL h<sup>-1</sup>, respectively. To form a stable and uniform core-sheath structure, the spinning rate of core layer solution was kept at lower flow rates than that of sheath layer solution. A high voltage of 21 kV was applied to spinneret and the collecting drum was rotated at 300–350 rpm. The PMIA/PAN-based coaxial nanofibers were collected on a polypropylene (PP) spun bond non-woven mat, which was rolled over the rotating cylindrical drum. All experiments were performed at about 30 °C in 60% relative humidity.

Thus produced PAN/PMIA coaxial nanofibers were integrated with PAN/Ag NP nanofibers to develop a multilayered filter with a stable cavity structure for application in air filtration of particulate and microbial contaminants.

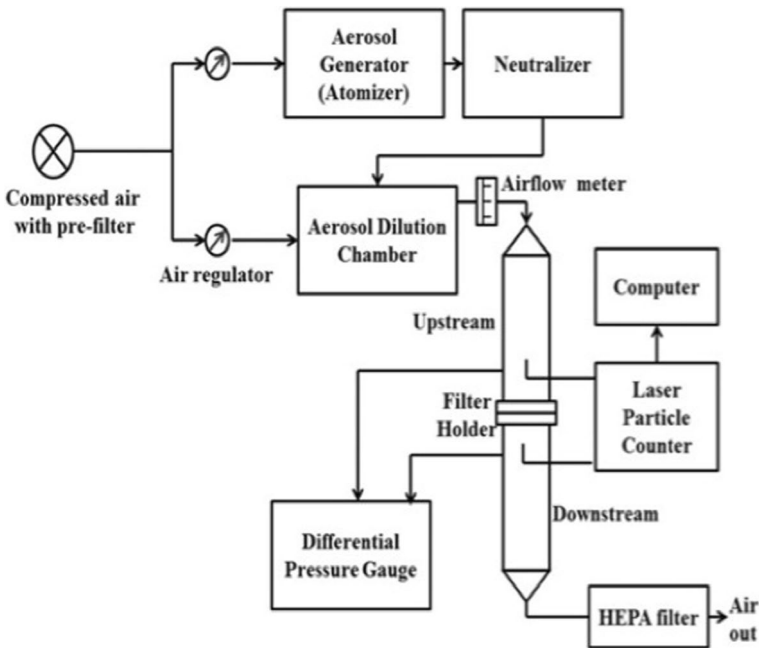


Fig. 3 Experimental setup for aerosol filtration efficiency tester

## Filtration efficiency tester

As shown in Fig. 3, the experimental setup for measuring air filtration efficiency (FE) of developed membrane was based on ASTM F2299. NaCl aerosols with size ranging from 0.3 to 3  $\mu\text{m}$  was generated as the challenge aerosol and it was passed through P-120 nebulizer. The developed NFM placed between PP nonwoven (with its inner circular diameter of 50 mm) was held together using a filter holder. Face velocity was maintained at 5 cm/s throughout the filtration test process. Lasair III-Particle Measuring System (a laser particle counter) was used to estimate the downstream and upstream particle count.

The FE is expressed as follows:

$$\text{FE \%} = [(C_{\text{upstream}} - C_{\text{downstream}}) / C_{\text{upstream}}] \times 100 \quad (1)$$

where  $C_{\text{downstream}}$  and  $C_{\text{upstream}}$  are the aerosol concentrations of the downstream and upstream air, respectively.

## Zone inhibition test for antimicrobial activity

The antibacterial activity of developed filters with and without Ag NPs was tested against Gram-positive *Bacillus subtilis* (*B. subtilis*) and Gram-negative *Escherichia coli* (*E. coli*) according to AATCC90 test method. Nutrient agar was poured in a petri dish and was kept under laminar airflow with UV germicidal lamp to prevent contamination of experiments. 50  $\mu\text{L}$  of microbial suspension (*B. subtilis* or *E. coli*) containing approximately  $1 \times 10^6$  CFU/mL of the test organism was streaked uniformly over the solidified agar; over which neatly cut NFM as test samples along with control (only PAN nanofibers with no Ag NP) were gently placed. The plates were then incubated for 24 h at 37  $^{\circ}\text{C}$ . The same procedure was carried out for both bacterial strains. The experiment was run in triplicate ( $n=3$ ) and the results produced by zone of inhibition are shown in Table 1.

## Bacterial filtration efficiency

The bacterial filtration efficiency was determined using Andersen sampler by testing the prepared filter medium according to ASTM F 2101:2019 using: *Staphylococcus aureus* (ATCC # 6538) as the test aerosol. The Anderson sampler essentially uses a multi-stage (six staged) impaction to collect 6 aerosol fractions on the perforated plate/growth medium, with air intake from the top. Six stage in the sense that the particle size is cascaded in six different categories. For instance, the particles with aerodynamic diameter larger than 7  $\mu\text{m}$  flow from top to the first stage, the second stage would have particles with aerodynamic diameter around 4 to 7  $\mu\text{m}$ , and the last category will be the smallest with size around 0.5–1.1  $\mu\text{m}$  impacting the agar. The flow rate during testing was 28.3 L/min (1  $\text{ft}^3/\text{min}$ ) and the mean particle size of challenge aerosol was in the range 0.3 to 3.0  $\mu\text{m}$ . The aerosol particles were pumped

**Table 1** Particulate and bacterial filtration efficiency, antimicrobial activity (values with mean  $\pm$  SD,  $n=3$ ) and other functional properties of developed nanofibrous membranes

Samples	Tensile strength (MPa)	Air permeability ( $\text{cm}^3/\text{cm}^2/\text{s}$ )	Pore size ( $\mu\text{m}$ )	Pressure drop (Pa)	Particulate filtration efficiency (%)	Antimicrobial activity (in mm)		Bacterial filtration efficiency (%)	
						Gram + ve			Gram - ve
						Gram + ve	Gram - ve		
PAN	1.91 $\pm$ 0.11	169.44 $\pm$ 0.15	2.71 $\pm$ 0.04	29.48 $\pm$ 1.43	94.88 $\pm$ 0.94	0	0	88.21 $\pm$ 1.46	
S3	1.68 $\pm$ 0.10	156.94 $\pm$ 0.16	2.45 $\pm$ 0.15	26.48 $\pm$ 0.91	94.96 $\pm$ 0.90	6.50 $\pm$ 0.50	6.60 $\pm$ 0.51	-	
S5	2.06 $\pm$ 0.29	165.77 $\pm$ 0.23	3.26 $\pm$ 0.34	24.50 $\pm$ 1.53	94.79 $\pm$ 1.01	9.50 $\pm$ 0.50	9.70 $\pm$ 0.57	-	
S7	2.36 $\pm$ 0.50	150.33 $\pm$ 0.42	2.39 $\pm$ 0.23	29.40 $\pm$ 1.34	94.88 $\pm$ 0.66	11.83 $\pm$ 0.76	11.50 $\pm$ 0.50	-	
S9	2.59 $\pm$ 0.53	156.94 $\pm$ 0.12	2.01 $\pm$ 0.07	30.47 $\pm$ 0.34	93.96 $\pm$ 0.96	11.73 $\pm$ 0.25	13.53 $\pm$ 0.75	-	
S11	3.84 $\pm$ 0.46	158.33 $\pm$ 0.13	1.34 $\pm$ 0.62	34.32 $\pm$ 1.05	95.90 $\pm$ 1.44	11.67 $\pm$ 0.28	13.50 $\pm$ 0.50	-	
S13	3.70 $\pm$ 0.59	154.41 $\pm$ 0.32	2.54 $\pm$ 0.23	36.28 $\pm$ 0.93	94.42 $\pm$ 0.89	13.50 $\pm$ 0.50	16.50 $\pm$ 0.50	-	
S15	3.02 $\pm$ 0.70	141.67 $\pm$ 0.41	1.78 $\pm$ 0.14	38.08 $\pm$ 0.75	96.10 $\pm$ 0.68	15.16 $\pm$ 0.76	17.50 $\pm$ 0.50	-	
S17	2.22 $\pm$ 0.71	144.44 $\pm$ 0.17	1.18 $\pm$ 0.17	39.22 $\pm$ 1.17	95.90 $\pm$ 1.12	15.00 $\pm$ 0.50	16.50 $\pm$ 0.50	-	
S19	2.19 $\pm$ 0.68	144.44 $\pm$ 0.37	1.05 $\pm$ 1.03	39.22 $\pm$ 0.87	96.32 $\pm$ 1.45	14.16 $\pm$ 0.76	16.17 $\pm$ 0.28	-	
PP-NW	-	458.30 $\pm$ 0.34	66.3 $\pm$ 0.16	0	32.05 $\pm$ 0.91	-	-	30.08 $\pm$ 1.66	
PAN/PMIA	10.47 $\pm$ 0.84	258.83 $\pm$ 0.24	5.24 $\pm$ 1.23	0	79.63 $\pm$ 1.19	-	-	72.67 $\pm$ 1.55	
NFM 1	12.09 $\pm$ 0.10	110.00 $\pm$ 0.52	0.23 $\pm$ 1.05	51.97 $\pm$ 2.01	99.30 $\pm$ 0.05	-	-	99.46 $\pm$ 0.72	
NFM 2	13.76 $\pm$ 0.47	97.22 $\pm$ 0.16	0.18 $\pm$ 0.93	53.93 $\pm$ 1.72	99.41 $\pm$ 0.31	-	-	99.51 $\pm$ 0.09	
NFM 3	13.63 $\pm$ 0.91	79.16 $\pm$ 0.24	0.16 $\pm$ 1.42	58.84 $\pm$ 2.81	99.37 $\pm$ 0.40	-	-	99.11 $\pm$ 0.82	

\*PP-NW polypropylene nonwoven, NFM1 PAN/PMIA coaxial NFM integrated with S13, NFM 2 PAN/PMIA coaxial NFM integrated with S15, NFM 3 PAN/PMIA coaxial NFM integrated with S17

and loaded in a nebulizer under a face velocity of 20 cm/s. The samples of *S. aureus* were kept for about 4 h at 21 °C and 85% relative humidity prior to testing, with 2260 CFU/mL as the yield level.

The sample was placed over a six-stage sampler through which the generated aerosol was passed. The bacterial aerosols impinge on the six stage agar plates, which were later incubated for 48 h at  $37 \pm 2$  °C. After which the formed colonies were counted. The bacterial filtration efficiency (BFE) was calculated as given in Eq. (2) [11].

$$\text{BFE \%} = \frac{C - T}{C} \times 100 \quad (2)$$

where  $C$  is the CFU/mL of control and  $T$  is the CFU/mL of the Test sample.

## Characterization techniques

Scanning electron microscope (SEM) was employed to observe the morphology and structure of nanofibers. High-resolution transmission electron microscopy (HR-TEM: Jeol/JEM 2100, Sophisticated Test & Instrumentation Centre, Cochin, India) operated at an accelerating voltage of 200 kV was used to study the morphology of PMIA/PAN nanofibers with core-shell structure. Image analytical software (Image J) was used to measure the diameters of nanofibers from SEM images. Air permeability tester was used to analyze permeability and to measure rate of airflow passing through the NFM according to ASTM D 737-04. The pore size of NFM was measured using a capillary flow porometer CFP-1200A (SITRA, Coimbatore, India). Instron (INSTRON 3369-UTM, US) with 100 N load cell was used to investigate the mechanical properties of membranes. The clamping distance was 20 mm and speed level was at  $5 \text{ mm min}^{-1}$ . The formation of Ag NP in PAN nanofibers was confirmed through Fourier transform infrared spectroscopy (FTIR), ultraviolet-visible (UV) spectroscopy (Hitachi U-2900), X-ray diffraction (XRD) and SEM with Energy-Dispersive X-Ray Analysis (EDX). The existence of Ag NPs in the nanofiber was further verified using X-ray photoelectron spectroscopy (XPS) (Thermo Scientific K-Alpha surface analysis). The thermodynamic property of PAN and PAN/ Ag NP NFM in order to quantify the silver incorporated inside fiber was evaluated using thermo gravimetric analysis (TGA).

## Results and discussion

### Membrane morphology and structure

Figure 4 shows the SEM images for PAN nanofibers with all the different wt.% of Ag NP. The fiber diameter analyzed from SEM images and the average diameter is represented as histogram in Fig. 4. The average diameter of pristine PAN nanofiber is noted to be 195 nm. The diameter of PAN/Ag NP fiber with  $\text{AgNO}_3$  concentration 3, 5, 7, 9, 11, and 13 wt.% decreased with an increase in Ag NP



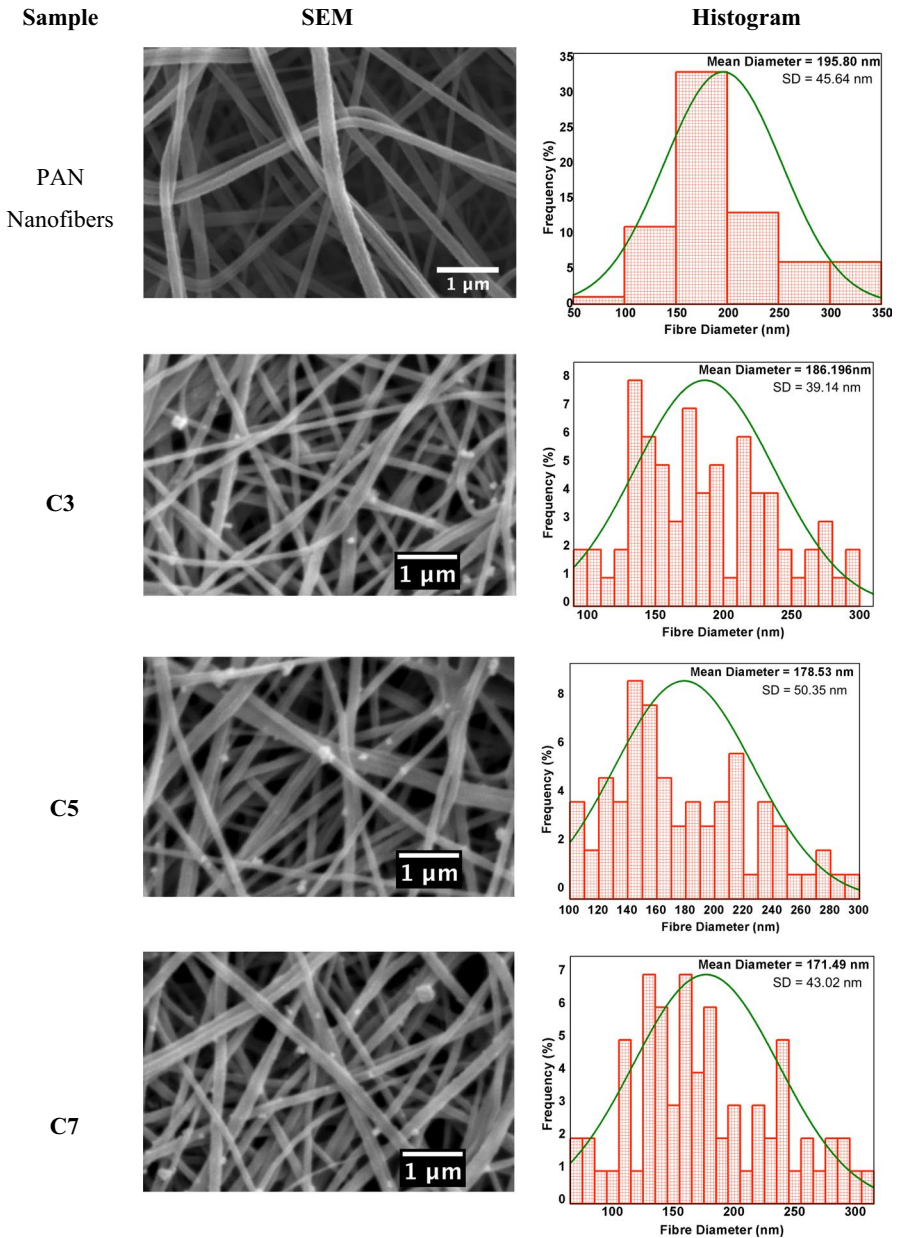


**Fig. 4** SEM images of the electrospun PAN nanofibers (8 wt.%) with Ag nanoparticles (3, 5, 7, 9, 11, 13, 15, 17 and 19 wt.% with respect to PAN) and their respective diameter distribution histogram

concentration in PAN solution. However, for PAN/Ag NP fiber with AgNO<sub>3</sub> concentration 15, 17 and 19 wt.% the diameter was increasing. The trend of reduction in fiber diameter is an indication of increase in charge density in polymeric

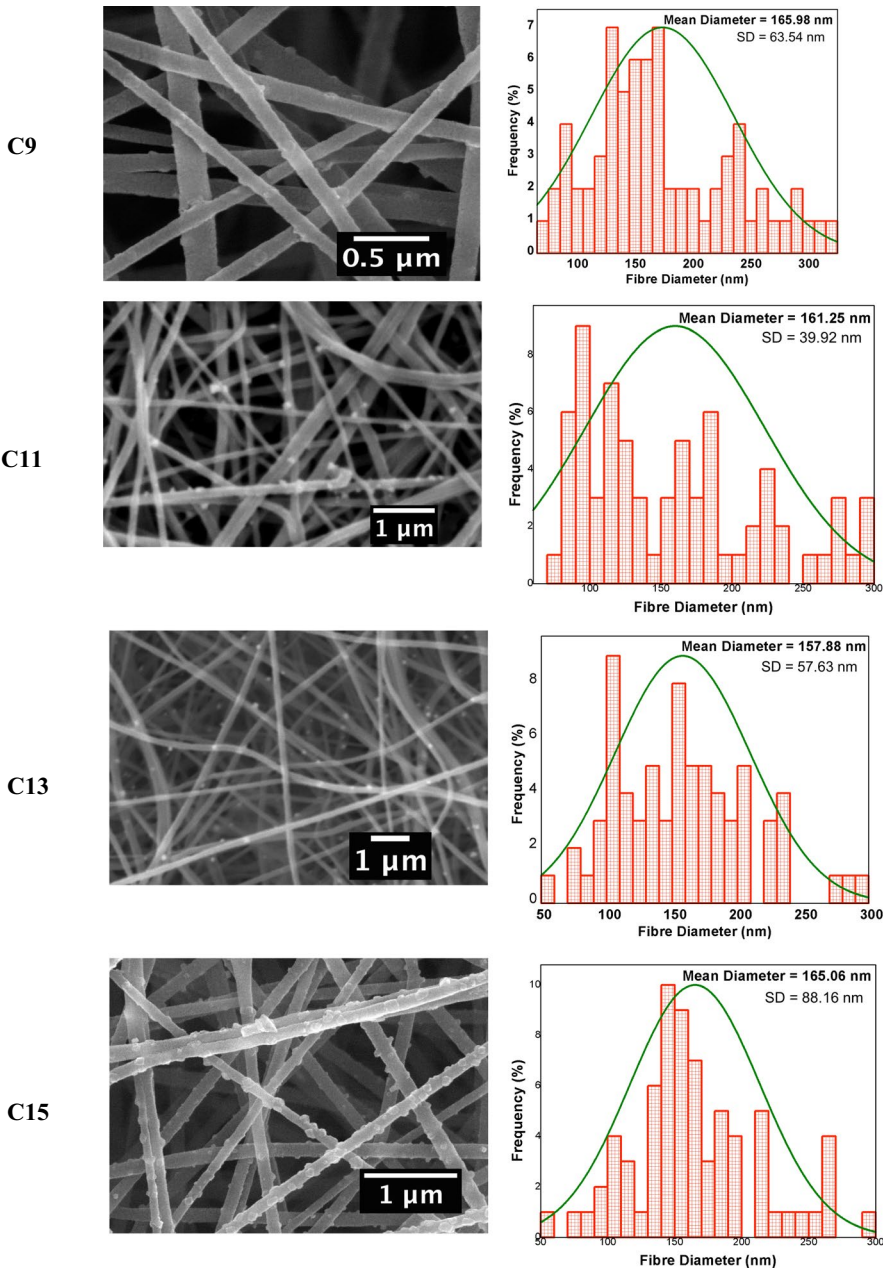


Fig. 4 (continued)

solution with an increase in Ag NP concentration. An increase in charge density in electrospinning solution will inflict a strong elongation force to the ejected polymeric jet while they travel from nozzle to collector under electrical field.

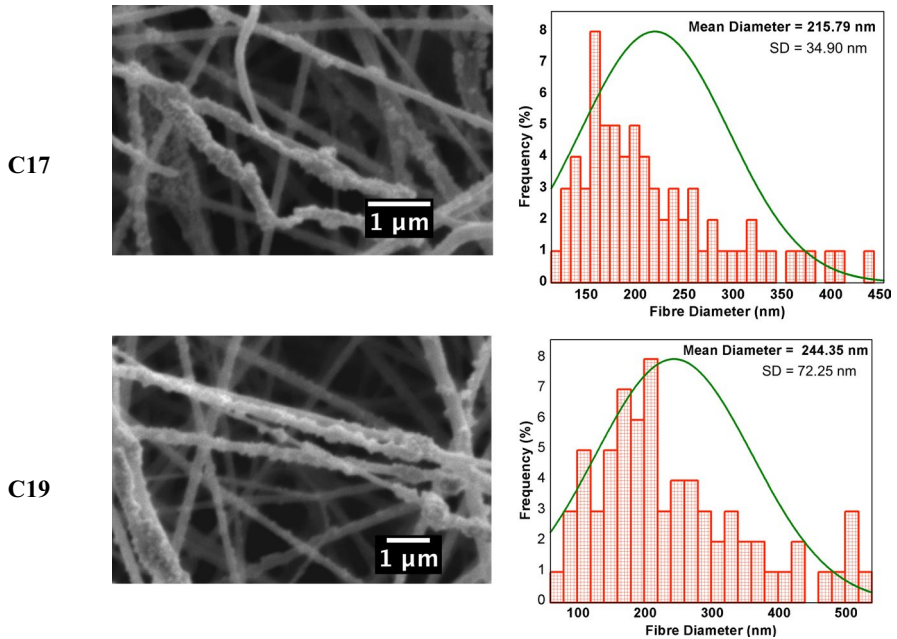


Fig. 4 (continued)

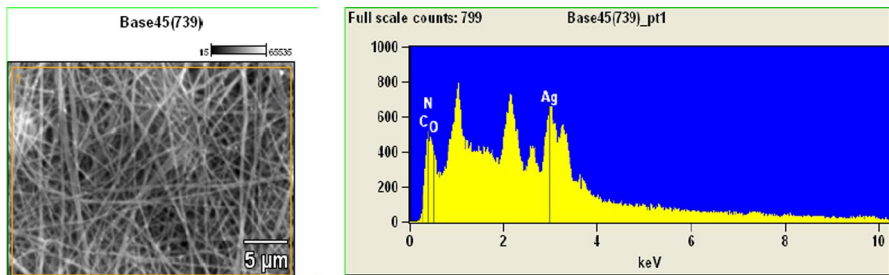
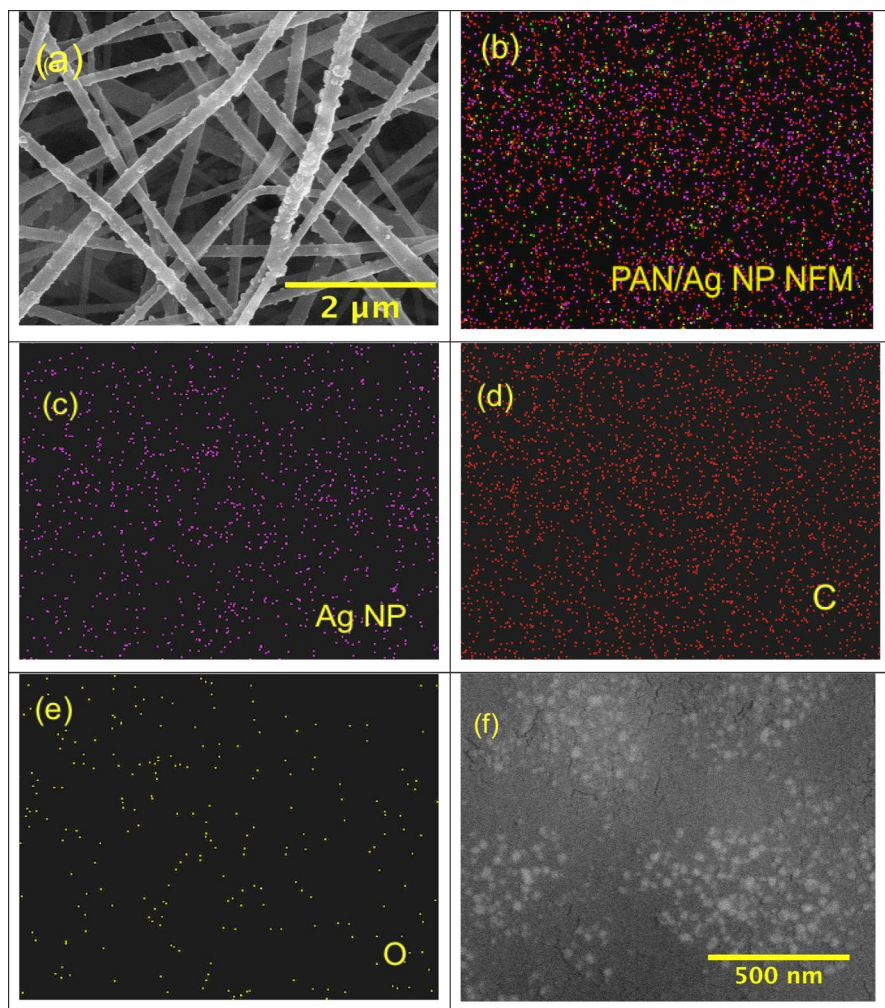


Fig. 5 The energy-dispersive spectrum (EDX) collected on the PAN/Ag NPs nanofibers

This results in a decrease in fiber diameter. However, with an increase in Ag wt.% over 13 wt.%, there is an increase in fiber diameter which is ascribed to the agglomeration of Ag NP over nanofibers.

Furthermore, the elemental composition of the Ag NPs-embedded PAN NFM was characterized using energy-dispersive X- ray spectroscopy (EDX) as shown in Fig. 5. This result confirmed the presence of Ag NPs in developed PAN NFM. Figure 6b–e shows the mapping of elements (Ag NP, C and O) on PAN/Ag NP NFM. The Ag NPs are distributed throughout the surface of nanofibers. Figure 6f shows the HR SEM image of Ag NP formed in PAN polymeric solution. The average particle size was noted to be  $32.47 \pm 42.57$  nm.



**Fig. 6** a HR SEM of PAN/Ag NP NFM; b–e Elemental mapping of the PAN/Ag NP NFM showing the distribution of all the elements, Ag NP, C, and O, respectively; f HR SEM image of the Ag NP formed in PAN polymeric solution

### XRD and UV analysis of PAN/Ag NP nanofibers

Generally, Ag NP synthesis from  $\text{AgNO}_3$  requires a strong reducing agent and a stabilizing agent. Stabilizing agent is essential to prevent agglomeration of the nanoparticles formed. In this work, DMF acted as a reducing agent in the formation of Ag NP and as a solvent for PAN. PAN acted as the stabilizing agent by preventing agglomeration and enabled a good dispersion of Ag NP in solution.

XRD diffraction pattern is analyzed to study the structural and crystalline behaviors of Ag NP on PAN NFM. The XRD patterns of various concentrations of Ag

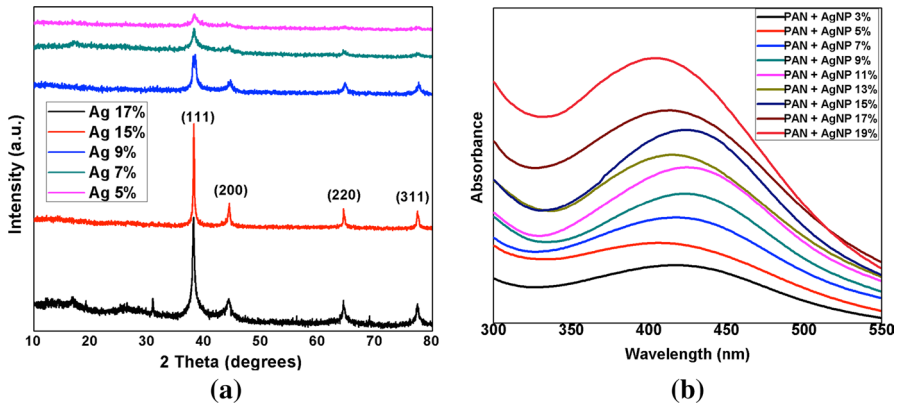


**Fig. 7** **a** XRD spectra of PAN nanofibers with Ag nanoparticles (5, 7, 9, 15 and 17 wt.%); **b** UV–visible spectroscopy of 9 samples with various Ag NP concentration in PAN solution

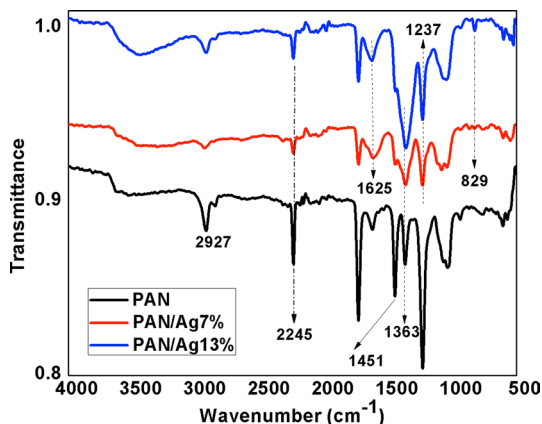
NP-embedded PAN nanofibers are presented in Fig. 7a. (111), (200), (220) and (311) are the Bragg’s reflections of fcc structure of Ag and is indicated by the characteristic peaks at 2theta=38, 44.5, 65.6, and 78.5, respectively. With an increase in concentration of Ag NP in PAN NFM matrix, the diffraction peak intensity becomes stronger. This also indicates that with incorporation of Ag NP, there is evident crystallization of PAN NFM.

Figure 7b shows the UV–visible spectra for PAN solution with 3, 5, 7, 9, 11, 13, 15, 17 and 19 wt.% of Ag NP. UV–Vis spectroscopy was used to determine the formation of Ag NP in the PAN/DMF solution. The electronic transitions of Ag + ion and metallic Ag (0) produce a characteristic absorption band situated around 200 nm and 250–330 nm, respectively [26]. Due to the discrete energy levels of electrons caused by the quantum size effect, nanometallic particles in general demonstrate high optical absorbance. Ag NP exhibits a strong absorption band centered from 410 to 420 nm. Despite the fact that the exact position of maximum absorption depends on dielectric constant and the shape of Ag NPs, spectra here is used to determine the formation of Ag NP in PAN/DMF polymeric solution. Figure 7b shows drastic changes in the absorption spectrum of a PAN solution with an increase in AgNO<sub>3</sub> wt.%. For samples (S3-S15), the peaks are centered at about 410–420 nm and there was an increase in intensity (indicates the increased formation of Ag NP) with increase in AgNO<sub>3</sub> wt.% in PAN/DMF solution. However, from Fig. 7b it is evident that samples S17 and S19 have peaks located below 400 nm, which indicates aggregation of nanoparticles.

### FTIR spectra of PAN/Ag NP

The FTIR spectra of electrospun pristine PAN nanofibers and PAN nanofibers with two different concentration of Ag NP (7, 13 wt.%) are shown in Fig. 8. For pristine PAN nanofibers, the characteristics peaks at 2927–2853.03 cm<sup>-1</sup>, 1451.01 cm<sup>-1</sup>, 1363.14 cm<sup>-1</sup>, 1237.94 cm<sup>-1</sup> can be assigned to aliphatic CH group (CH, CH<sub>2</sub>, and

**Fig. 8** FTIR spectra of the PAN nanofiber and PAN nanofibers with Ag NPs (7 and 13 wt.%)



CH<sub>3</sub>) vibrations. The presence of amide groups in PAN can be shown through a weak peak at 1625.97 cm<sup>-1</sup>, while another peak around 1660 cm<sup>-1</sup> can be ascribed to C=O bond, which is an indication of trace DMF present in PAN nanofibers by virtue of incomplete solvent evaporation. The absorption peak at 2245.72 cm<sup>-1</sup> and 3500 cm<sup>-1</sup> can be ascribed to C≡N (nitrile group) and stretching vibration of hydroxyl group respectively. These peaks have appeared in all three-sample spectra. However, it can be noted that the position of the characteristic peak at 2927.68 cm<sup>-1</sup> in case of PAN/Ag NP 7 and 13% have shifted to lower values. Apparently this is due to an interaction between PAN molecules and Ag NP. Significantly, we can observe a new set of peak emerging for PAN/Ag NP 7 and 13% at 829 cm<sup>-1</sup>, which can be attributed to N–O stretching and bending vibration of nitrate ions from AgNO<sub>3</sub> (residual silver salt on PAN nanofibers). Also, in Fig. 8 there is an evident rise of the band at 3400–3500 cm<sup>-1</sup>, which can be ascribed to the newly formed hydroxyl groups on PAN nanofibers. Presumably, with the incorporation of Ag NP onto PAN nanofibers, moisture absorption would have been promoted over the highly reactive Ag NP surface. This validates the rising hydroxyl peak with the Ag NP based PAN nanofibers. After Ag NPs developed on the surface of nanofibers; some moisture would have gotten absorbed on the highly reactive surfaces of Ag NPs. The existence of absorbed water validated the rising hydroxyl peaks in the case of PAN/Ag NPs. This indicates the successful formation of Ag NPs on PAN nanofibers.

More significantly, it must be noted that there is no evident shift in peak 2245 cm<sup>-1</sup> corresponding to C≡N nitrile group, implying no possibility for formation of coordination bonds between PAN and silver [27]. However, in the presence of silver ions the nitrile groups in PAN might have been polymerized, thus decreasing the number of C≡N present in the PAN chain as shown in Fig. 9.

### X-ray photoelectron spectroscopy of PAN and PAN/Ag NP nanofibrous membrane

XPS spectra were examined in order to verify further the in situ production of Ag NP in PAN NFM. Wide scan spectra in the binding energy range 200–800 eV with Ag 3d XPS spectra are displayed in Fig. 10. After in situ reduction of Ag, the

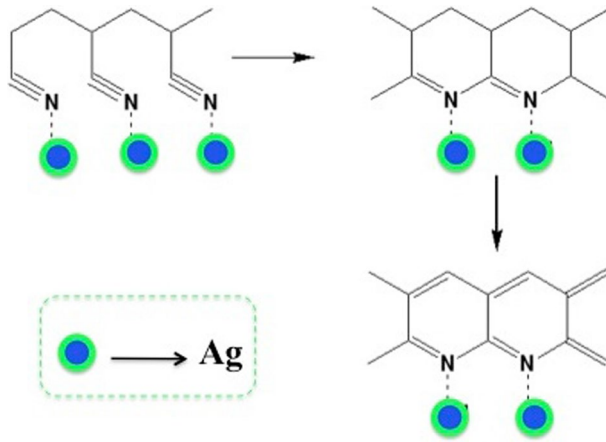


Fig. 9 The chemical reaction mechanism of Ag NPs with PAN nanofibers

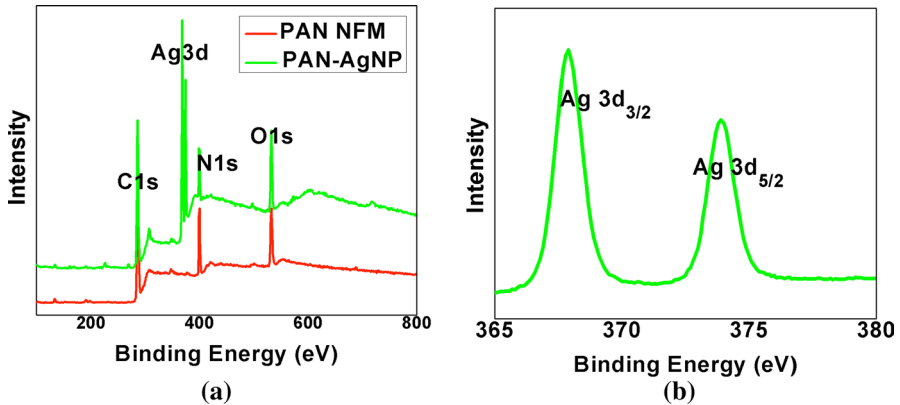


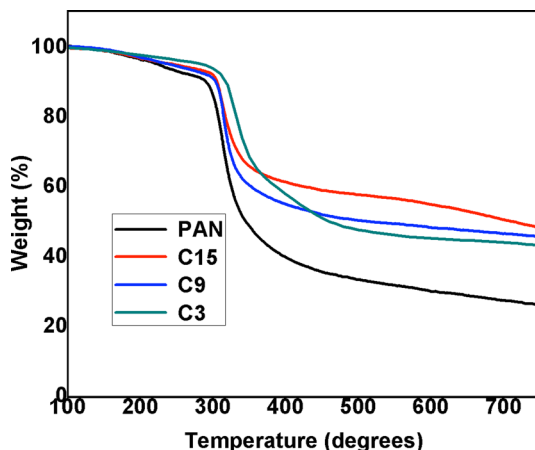
Fig. 10 XPS spectra of electrospun PAN and PAN/Ag NP NFM **a** wide-scan spectra; **b** Ag3d doublet peaks assigned to binding energies  $3d_{5/2}$  and  $3d_{3/2}$

existence of doublet peaks in the Ag 3d spectra for PAN/Ag NP NFM, together with peaks of C 1s, N 1s, and O 1s, demonstrates that silver was successfully absorbed into the PAN nanofibers. Ag NPs produced in PAN NFM have doublet peaks at 372.7 eV and 366.5 eV, respectively, with 6.2 eV gap between core levels, indicating the presence of oxidized species of Ag.

### Thermogravimetric analysis of PAN and PAN/Ag NP nanofibrous membrane

TGA of PAN NFM, PAN/ Ag NP NFM developed with using 3, 9 and 15 wt-% of  $AgNO_3$ , namely C3, C9 and C15 samples were carried out at a heating rate of 20 °C/min, with temperature sweep ranging from 0 to 700 °C under nitrogen atmosphere. Figure 11 shows the obtained TGA curves for all 4 NFMs. Due to moisture and

**Fig. 11** TGA of PAN, PAN/Ag NP (3 wt.%; C3), PAN/Ag NP (9 wt.%; C9) and PAN/Ag NP (15 wt.%; C15)



solvent loss, there is little weight loss around 100–250 °C. The primary mass loss began about 300 °C, due to the polymeric nanofibrous membrane pyrolysis. Above 350 °C, the curve for PAN dips significantly, indicating that the sample is degrading quickly. However, it can be noted that for the samples C3, C9 and C15, the incorporated silver nanoparticles helped to marginally improve the thermal stability of PAN nanofibrous membranes.

The incorporated Ag NP in PAN NFM is calculated using Eq. (3). This method compares the final charred residue of both unmodified and modified PAN NFM, utilizing the difference in mass loss at 700 °C.

$$\text{Incorporated Ag NP (mmol/g)} = \left( W_{\text{res}\%} / M_{w_{\text{AgNO}_3}} \right) \times 1000 \quad (3)$$

where,  $W_{\text{res}\%}$  corresponds to percentage of residual Ag at 700 °C for each of the samples (C3, C9 and C15), and  $M_{w_{\text{AgNO}_3}}$  is the molar mass of  $\text{AgNO}_3$ . The incorporated AgNP in PAN NFM according to the formula given in Eq. (3) is obtained as 0.19, 0.72, and 1.46 mmol/g for C3, C9 and C15, respectively. The result shows that Ag NP loading increased with increasing the  $\text{AgNO}_3$  concentration in PAN polymeric solution.

### Anti-microbial property of PAN/Ag NP nanofibrous membrane

Zone of inhibition for electrospun PAN/Ag NP (various wt.%) NFM was tested against *E. coli* and *B. subtilis*, where pristine PAN was applied as the control. As shown in Fig. 12, it can be observed that no zone was formed around pure PAN towards both gram-positive and negative species. The in situ addition of Ag NP to PAN NFM imparted a clear zone of inhibition around the membranes. An increase in Ag NP concentration in PAN solution resulted in gradual increase in bactericidal activity, which is attributed to the antibacterial property of Ag NP. The bacterial growth is inhibited with bacterial cell wall degradation, when the



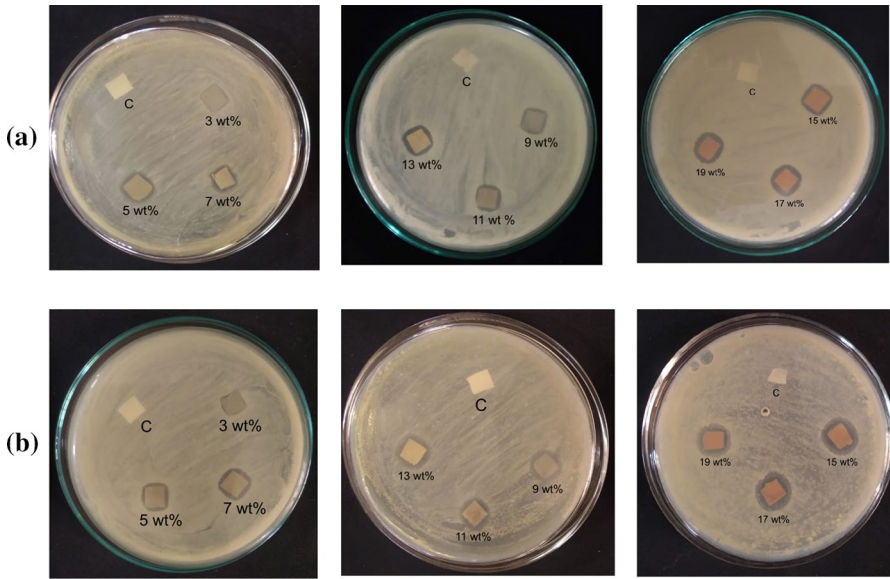


**Fig. 12** Zone of inhibition of prepared PAN/Ag NP against **a** *B. subtilis* and **b** *E. coli*

test organisms (especially its negatively charged bacterial cell wall) interact with the antimicrobial components of Ag NP.

Integrated NFM placed between PP-nonwoven were developed after testing the PAN/Ag NP samples (S1-S9) for their antimicrobial activity. From Fig. 12 and Table 1, it is evident that 13, 15, and 17-wt.% of Ag NP exhibited good antibacterial activity and tensile strength when compared to rest of the samples. Hence, S13, S15 and S17 were integrated with PAN/PMIA based uniaxially aligned NFM to form three separate NFMs namely NFM1, NFM 2 and NFM 3.

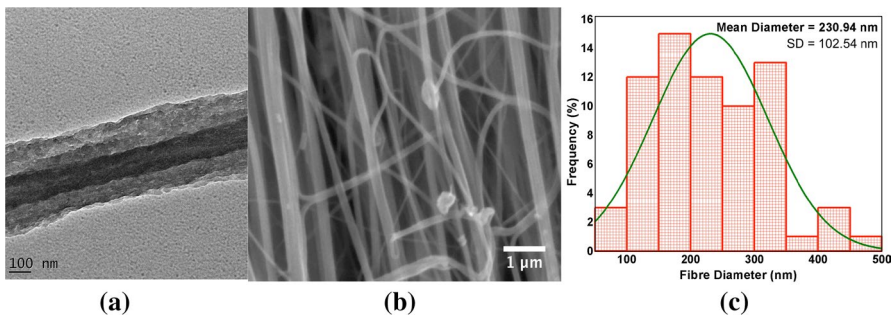


**Fig. 13** **a** TEM; and **b** SEM images of electrospun coaxial PMIA/PAN nanofibers

## Morphology of PAN/PMIA based coaxial nanofibrous membrane

The TEM and SEM images of electrospun PMIA/PAN coaxial nanofibers collected on PP non-woven is shown in Fig. 13. In the TEM image, the core–shell structure is evident with core PMIA as the darker area and shell PAN as the lighter area. The contrast connecting core and shell is quite notable; implying the immiscibility of two polymeric solutions considered for coaxial electrospinning or could be due to the fast electrospinning that prevented mixing of solutions. Nevertheless, the choice of polymer and solvent system is very important while electrospinning coaxial nanofibers. This is due to the fact that core polymeric solution should not precipitate and clog the spinneret nozzle when in contact with shell polymeric solution and vice-versa. The SEM image reveals the uniaxial alignment of PMIA/PAN coaxial nanofibers with average fiber diameter of  $230.94 \pm 102.54$  nm.

Considering our previous work [28], it is clear that the tip-to-collector distance is one of the most important parameters since it influences diameter of electrospun fibers and has a significant impact on whipping path of jet thus influencing fiber deposition pattern as well. This would change the filtration and tensile properties of nanofibrous membrane to a large extent. Compared to our previous work (where the average fiber diameter of PAN/PMIA coaxial nanofibers were around 300 nm when the distance of 20 cm was kept between nozzle tip and the collector) the present work exhibited lower fiber diameters of approximately  $230.94 \pm 102.54$  nm [28]. While we discuss this, one important fact to be noted is that a minimum nozzle-collector distance is essential to give enough time for drying of solvent from the ejected polymeric jet before it can be collected on collector and solidify. The distance should not be too short or too far in order to avoid bead formation. Although compared with other processing conditions, the nozzle tip-to-collector distance is less significant in determining fiber diameter and other properties; in the present work while electrospinning PMIA/PAN coaxial nanofibers we found a huge impact of the distance on produced NFM. The NFM produced with a reduced tip-to-collector distance (10 cm) had a great impact on the tensile strength (as shown in Table 2) because of the fiber deposition pattern.

## Mechanical properties of PAN and PAN/PMIA based integrated nanofibrous membrane

From Table 1, we can see that the average breaking strength of pristine PAN and PAN/Ag NFM is around  $1.91 \pm 0.11$  to  $3.84 \pm 0.46$  MPa. The average breaking strength of the PAN/Ag NP NFM when integrated with coaxial PMIA/PAN fibrous membrane were effectively enhanced from  $\sim 3$  MPa to  $13.76 \pm 0.47$  MPa (for NFM2) owing to the inherent reinforcing ability of PMIA polymer considered for electrospinning. The results show that under initial tensile force, the NFM showcases a nonlinear elastic deformation as single nanofibers oriented along stress direction breaks under the action of tensile force until NFM itself breaks and returns to a zero strain state. Lu Zhang et al. explored a simple and effective method to fabricate

**Table 2** A few earlier reported nanofibrous membranes for aerosol and bacterial filtration

S.no	Polymer nanofibers	Nozzle-col-lector distance (cm)	Pressure drop (Pa)	Tensile strength (MPa)	PFE (%)	BFE (%)	Reference, year
1	PVA/poly (acrylic acid) (PAA)/hydrophobic silica NPs/Ag NPs	12	150	8.74	–	98	[31], 2018
2	Cellulose	13	–	–	–	87.5	[32], 2018
3	Mesoporous titanium dioxide (TiO <sub>2</sub> ) beads/PAN	15	88	–	96.75	–	[33], 2019
4	Ag Doped Keratin/Polyamide-6	25	140	–	–	96.8	[34], 2019
5	PAN/Ag	15	68	~4	> 98.65	–	[35], 2019
6	TiO <sub>2</sub> /PAN, Ag/PAN, Zinc Oxide (ZnO)/PAN	15	68–183.47	–	> 97–100	–	[36], 2019
7	PVA/chitosan/3-allyl-5, 5-dimethylhydantoin	20	183	6.1	99.3	99.4	[37], 2020
8	Cotton-polylactic acid-cotton	18	35.78	–	–	97.9	[38], 2021
9	Ag-loaded PAN/PVDF composite	15	~100	4.13	93.91	99.2	[39], 2021
10	Metal-organic framework/PAN	17	53	–	95.1	97.4	[40], 2021
11	PVA/Ag NP	20	59	–	99.6	–	[41], 2021
12	ZnO NP/Ag NP/PAN	15	~200	–	80	–	[6], 2021
13	PMIA (8 wt.%)/PAN (10 wt.%) NFM with PAN/Ag NP	20	24.52	9.81	99.0	–	Previous Work, [29], 2021
14	PMIA (8 wt.%)/PAN (8 wt.%) coaxial NFM integrated with PAN/Ag NP	10	53.93	13.76	99.41	99.5	This Research Work

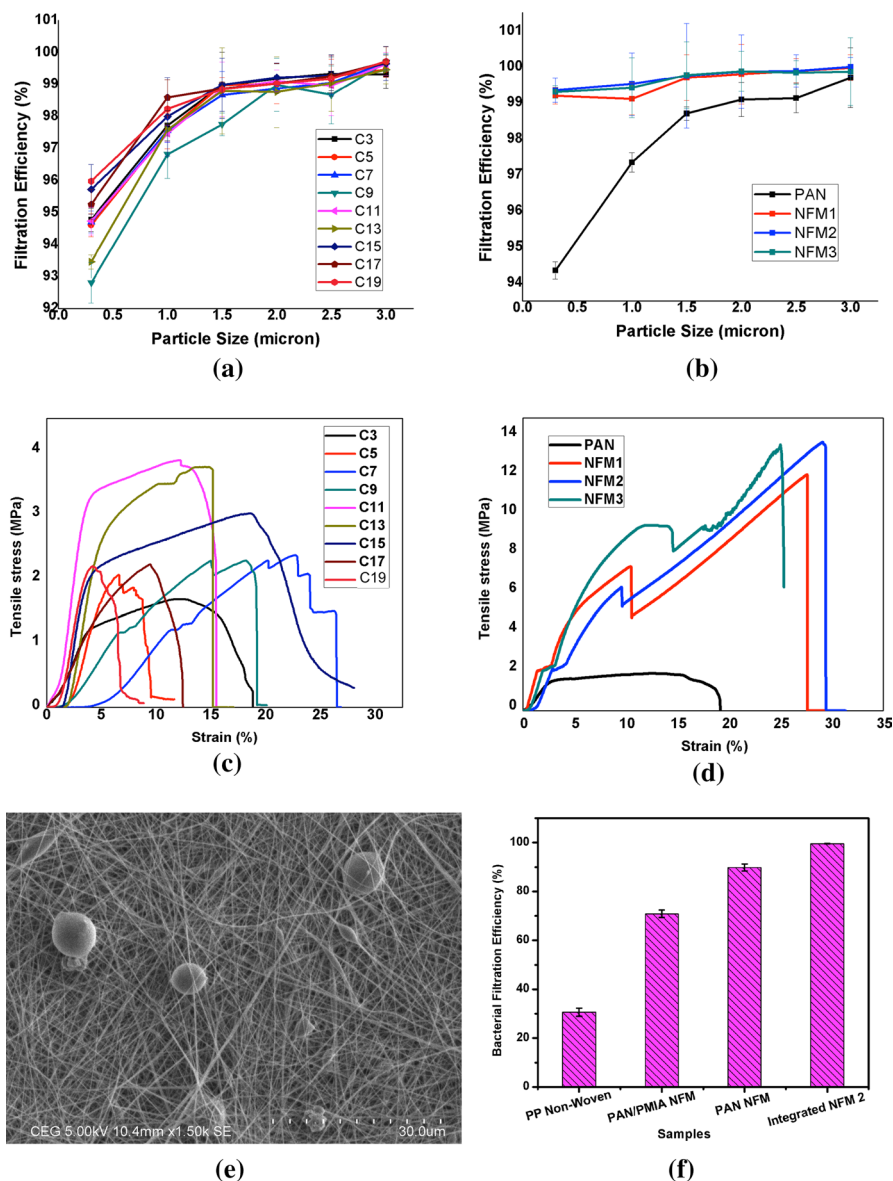


**Fig. 14** **a, b** Filtration efficiency of developed membranes with respect to aerosol size; **c, d** their respective tensile strength; **e** The PAN/Ag NP based integrated NFM after filtration; **f** bacterial filtration efficiency of PP nonwoven, Pristine PAN NFM, PAN/PMIA coaxial NFM, and NFM 2. The error bars represent standard deviation in each efficiency value reported ( $n=3$ )

multilayered PVA/Chitosan and PVA/ N-halamine biopolymer nanofibrous composite membrane with antibacterial property for air filtration. Those membranes displayed tensile strength of 6.1 MPa [37].

Besides, we have investigated PAN nanofibers with different concentration loads of Ag NPs. It was analyzed that pristine PAN nanofibers had the breaking strength of 1.914 MPa while for PAN/Ag NPs nanofibers the breaking strength increased initially. However, the strength decreased after a certain increase in Ag NP concentration as shown in Fig. 14c, d. With appropriate increase in concentration of AgNO<sub>3</sub> content, the intensification in tensile property is evident, which is again possibly related to excellent crystallinity of Ag NP. From Fig. 7a, with an increase in embedded Ag NPs in PAN nanofibers, the crystallinity of nanofibers increased as well. According to Ming He et al., the interfacial interaction between nanoparticle and the nanofibrous matrix increased with an increase in Ag NP content. Therefore, during the tensile deformation, there could have been a transfer of load from nanofibrous matrix to the dispersed Ag NPs to a certain degree. While the Ag NP content in polymer matrix increased after a certain concentration level, it could be due to the aggregation of abundant Ag NPs over and within the nanofiber matrix causing some amount of destruction in regularity of nanofibers (hindering proper orientation of polymer molecules). Hence a decrease in tensile property and elongation-at-break can be observed as in Fig. 14d [29].

### **Filtration performance of PAN/Ag NP and PAN/PMIA based integrated nanofibrous membrane**

According to standards of CNS 14774-2018 specification for medical facemasks, the bacterial filtration efficiency (BFE) must be > 95%. As given in Table 1, all the developed integrated NFM (NFM1, NFM2, NFM3) shows BFE > 95%, which indicate its high desirability for practical applications. Moreover, particulate filtration efficiency (PFE) and BFE of a filter are very important factors to be considered for practical applications [30]. Pore size of the developed filter membrane is a major factor in determining air permeation, pressure drop and finally filtration efficiency of the media. In this work as shown in Fig. 14, the 90 min electrospun PAN nanofibers display pore size ranging from 1 to 3 μm. Thus, pressure drop values and filtration efficiency will be low when compared to integrated NFM. When PAN/ Ag NP NFM is integrated with uniaxially aligned PMIA/PAN based coaxial nanofibers, there is a decrease in pore size, which was favorable to entrap particulate matter and the microbes with size below 2 μm. Due to smaller pore size, the filtration efficiency of integrated NFM (NFM1, NFM2, NFM3) is significantly higher. From Fig. 13a, b it can be noted that pure PAN and PAN/Ag samples (S1–S9) show good overall filtration efficiency, however filtration efficiency toward 0.3 μm particle is < 95%. When the PAN/Ag NP-based samples were integrated with PAN/PMIA NFM, the membranes (NFM, NFM2, NFM3) could filter 0.3 μm particles with excellent filtration efficiency of 99%. This is the result of smaller cavity structures created when integrating fibrous membranes together forming multiple layers.

The smaller pore size of integrated NFM is attributed to an increase in the packing density of nanofibers. Moreover, the multi-layering provides a stable cavity structure for multilevel physical sieving. Air permeability factor depends on the pore size of NFM. Hence, bigger the pore size, higher is the air permeability for a

filter and lower is the pressure drop. However, higher pore size will result in a filter medium displaying lower filtration efficiency. Here in this work, the filter was constructed in such a way that PP nonwoven and PMIA/PAN NFM did not contribute much to an increase in the pressure drop. While the layers are integrated together, the pore size is reduced to induce higher filtration efficiency at a low-pressure drop, which is again within the acceptable pressure drop limits. In fact, according to EN 14683:2019 (European standard for medical facemasks), the pressure drop that determines the breathability of a filter should be around 40–60 Pa.

Other than filtration performances, the stability of NFMs after filtration is one of the important parameters to be checked after its use as a filter medium. Figure 14e shows the SEM image of NFM after filtering the NaCl aerosol particles (indicated by spherical particles in the SEM image). We can observe that the structural integrity of the delicate nanofibrous membrane is retained well even after filtration. This shows that the developed NFM is satisfactorily stable.

Table 2 showcases a comparison to the present work with certain earlier reported NFM used for bacterial filtration application. It can be seen that Ag NP based NFM have been developed previously considering the superior and long lasting antimicrobial activity of silver nanoparticle in any polymer matrix. However, a hierarchically bi-layered integrated NFM (a layer of PAN/Ag NP and a layer of uniaxial aligned PAN/PMIA based coaxial NFM) as discussed here in this work can evidently resolve the typical bottleneck problem owing to a membrane's multi-functionality and its ability to achieve high filtration efficiency at a low pressure drop while retaining the vital tensile characteristics of the NFM. The majority of earlier research shows noticeably high filtration efficiency, however they either show larger pressure drop or have low tensile property or would not have successfully integrated multi-functionality into one membrane.

## Conclusion

In this work, a multifunctional composite NFM was designed by stacking up PMIA/PAN coaxial NFM with PAN/Ag NP membrane through electrospinning process. The results show that Ag NP was highly dispersed on the surface of PAN nanofibers and when integrated to PAN/PMIA NFM, did not only endow the filter medium with high bacterial filtration efficiency but also further improved particulate filtration efficiency of the composite membrane. PMIA was chosen due to its rigidity. Incorporation of PMIA in the core of PAN NFM through coaxial electrospinning enabled the resultant composite membrane to display promising mechanical strength.

In fact, coaxial NFM developed through coaxial electrospinning has exploited the properties of two different polymers, and the as-prepared uniaxially aligned PMIA/PAN nanofibers integrated with a layer of randomly oriented PAN/Ag NP nanofibers displayed intriguing mechanical strength of 13.76 MPa, which is very high when compared to PAN/Ag NP NFM (~ 3 MPa). This integrated structure also contributed to providing a stable cavity structure to adsorb not only PM<sub>0.3–2.5</sub> with 99.41% efficiency but also the microbes effectively (BFE = 99.51%).

**Acknowledgements** The authors gratefully acknowledge the support from the Council of Scientific & Industrial Research (CSIR), New Delhi, India, to carry out this research work successfully. (Sanction number—09/468/(0535) 2019 EMR—I).

**Code availability** Not applicable.

## Declarations

**Conflict of interest** There are no conflicts to declare.

**Consent to participate** Both the authors give their consent to participation.

**Consent to publication** Both the authors give their consent for the publication.

**Ethical approval** Not applicable.

## References

1. Zhu M, Han J, Wang F, Shao W, Xiong R, Zhang Q, Pan H, Yang Y, Samal SK, Zhang F, Huang C (2017) Electrospun nanofibers membranes for effective air filtration. *Macromol Mater Eng* 302:1600353. <https://doi.org/10.1002/mame.201600353>
2. Zhang R, Liu C, Hsu P, Zhang C, Liu N, Zhang J, Ryoung Lee H, Lu Y, Qiu Y, Chu S, Cui Y (2016) Nanofiber air filters with high-temperature stability for efficient PM<sub>2.5</sub> removal from the pollution sources. *Nano Lett* 16:3642–3649. <https://doi.org/10.1021/acs.nanolett.6b00771>
3. Robert B, Nallathambi G (2020) A concise review on electrospun nanofibres/nanonets for filtration of gaseous and solid constituents (PM<sub>2.5</sub>) from polluted air. *Colloids Interface Sci Commun* 37:100275. <https://doi.org/10.1016/j.colcom.2020.100275>
4. Nallathambi G, Robert B, Esmeralda SP, Kumaravel J, Parthiban V (2020) Development of SPI/AC/PVA nano-composite for air-filtration and purification. *Res J Text Appar* 24:72–83. <https://doi.org/10.1108/RJTA-09-2019-0044>
5. Karabulut FNH, Höfler G, Ashok Chand N, Beckermann GW (2021) Electrospun nanofibre filtration media to protect against biological or nonbiological airborne particles. *Polym* 13:3257. <https://doi.org/10.3390/polym13193257>
6. Ji M, Tiwari AP, Oh HJ, Kim HY (2021) ZnO/Ag nanoparticles incorporated multifunctional parallel side by side nanofibers for air filtration with enhanced removing organic contaminants and antibacterial properties. *Colloids Surf A Physicochem Eng Asp* 621:126564. <https://doi.org/10.1016/j.colsurfa.2021.126564>
7. Su J, Yang G, Cheng C, Huang C, Xu H, Ke Q (2017) Hierarchically structured TiO<sub>2</sub>/PAN nanofibrous membranes for high-efficiency air filtration and toluene degradation. *J Colloid Interface Sci* 507:386–396. <https://doi.org/10.1016/j.jcis.2017.07.104>
8. Sharma A, Kumar SR, Katiyar VK, Gopinath P (2021) Graphene oxide/silver nanoparticle (GO/AgNP) impregnated polyacrylonitrile nanofibers for potential application in air filtration. *Nano-Struct Nano-Objects* 26:100708. <https://doi.org/10.1016/j.nanoso.2021.100708>
9. Geltmeyer J, Teixeira H, Meire M, Acker TV, Deventer K, Vanhaecke F, Hulle SV, Buysser KD, Clerck KD (2017) TiO<sub>2</sub> functionalized nanofibrous membranes for removal of organic (micro)pollutants from water. *Sep Purif Technol* 179:533–541. <https://doi.org/10.1016/j.seppur.2017.02.037>
10. Victor FS, Kugarajah V, Bangaru M, Ranjan S, Dharmalingam S (2021) Electrospun nanofibers of polyvinylidene fluoride incorporated with titanium nanotubes for purifying air with bacterial contamination. *Environ Sci Pollut Res* 28:37520–37533. <https://doi.org/10.1007/s11356-021-13202-3>
11. Hirai H, Nakao Y, Toshima N (1979) Preparation of colloidal transition metals in polymers by reduction with alcohols or ethers. *J Macromol Sci: Part A - Pure Appl Chem* 13:727–750. <https://doi.org/10.1080/00222337908056685>
12. Yonezawa T, Toshima N (1992) Polymer- and micelle-protected gold/platinum bimetallic systems: preparation, application to catalysis for visible-light-induced hydrogen evolution, and

- analysis of formation process with optical methods. *J Mol Catal* 83:167–181. [https://doi.org/10.1016/0304-5102\(93\)87017-3](https://doi.org/10.1016/0304-5102(93)87017-3)
13. Guo-wen HE, Fen-fang LI, Jie-bin WEN, Cent J (2015) DMAc used as a reducer for preparation of spherical silver nanoparticles with high dispersion. *J Cent South Univ* 22:445–449. <https://doi.org/10.1007/s11771-015-2541-7>
  14. Santos IP, Serra-Rodríguez C, Liz-Marzán LM (2000) Self-assembly of silver particle monolayers on glass from Ag<sup>+</sup> solutions in DMF. *J Colloid Interface Sci* 221:236–241. <https://doi.org/10.1006/jcis.1999.6590>
  15. Pan SF, Ke XX, Wang TY, Liu Q, Zhong LB, Zheng YM (2019) Synthesis of silver nanoparticles embedded electrospun PAN nanofiber thin-film composite forward osmosis membrane to enhance performance and antimicrobial activity. *Ind Eng Chem Res* 58:984–993. <https://doi.org/10.1021/acs.iecr.8b04893>
  16. Karthick SA, Gobi N (2017) Nano silver incorporated electrospun polyacrylonitrile nanofibers and spun bonded polypropylene composite for aerosol filtration. *J Ind Text* 46:1342–1361. <https://doi.org/10.1177/1528083715622428>
  17. Liu B, Zhang S, Wang X, Yu J, Ding B (2015) Efficient and reusable polyamide-56 nanofiber/nets membrane with bimodal structures for air filtration. *J Colloid Interface Sci* 457:203–211. <https://doi.org/10.1016/j.jcis.2015.07.019>
  18. Cha D, Kim KW, Chu GH, Kim HY, Lee KH, Bhattarai N (2006) Mechanical behaviors and characterization of electrospun polysulfone/polyurethane blend nonwovens. *Macromol Res* 14:331–337. <https://doi.org/10.1007/BF03219090>
  19. Nimmanpipug P, Tashiro K, Rangsiman O (2006) Factors governing the three-dimensional hydrogen-bond network structure of poly(m-phenylene isophthalamide) and a series of its model compounds (4): similarity in local conformation and packing structure between a complicated three-arm model compound and the linear model compounds. *J Phys Chem B* 110:20858–20864. <https://doi.org/10.1021/jp062058r>
  20. Matulevicius J, Kliucininkas L, Prasauskas T, Buivydiene D, Martuzevicius D (2016) The comparative study of aerosol filtration by electrospun polyamide, polyvinyl acetate, polyacrylonitrile and cellulose acetate nanofiber media. *J Aerosol Sci* 92:27–37. <https://doi.org/10.1016/j.jaerosci.2015.10.006>
  21. Gobi N, Vijayalakshmi E, Berly R, Srinivasan NR (2018) Development of PAN nano fibrous filter hybridized by SiO<sub>2</sub> nanoparticles electret for high efficiency air filtration. *J Polym Mater* 35:317. <https://doi.org/10.32381/JPM.2018.35.03.6>
  22. Robert B, Nallathambi G (2021) Indoor formaldehyde removal by catalytic oxidation, adsorption and nanofibrous membranes: a review. *Environ Chem Lett* 19:2551. <https://doi.org/10.1007/s10311-020-01168-6>
  23. Chen K, Zhang S, Liu B, Mao X, Sun G, Yu J, Al-Deyab SS, Ding B (2014) Large-scale fabrication of highly aligned poly(m-phenylene isophthalamide) nanofibers with robust mechanical strength. *RSC Adv* 4:45760. <https://doi.org/10.1039/c4ra07901a>
  24. Lin CE, Wang J, Zhou MY, Zhu BK, Zhu LP, Gao CJ (2016) Poly(m-phenylene isophthalamide) (PMIA): a potential polymer for breaking through the selectivity-permeability trade-off for ultra-filtration membranes. *J Membr Sci* 518:72–78. <https://doi.org/10.1016/j.memsci.2016.06.042>
  25. Chen Y, Qiu L, Ma X, Chu Z, Zhuang Z, Dong L, Du P, Xiong J (2020) Electrospun PMIA and PVDF-HFP composite nanofibrous membranes with two different structures for improved lithium-ion battery separators. *Solid State Ion* 347:115253. <https://doi.org/10.1016/j.ssi.2020.115253>
  26. Venkatesham M, Ayodhya D, Madhusudhan A, Kumari AS, Veerabhadram G, Mangatayaru KG (2014) A novel green synthesis of silver nanoparticles using Gum Karaya: characterization, antimicrobial and catalytic activity studies. *J Clust Sci* 25:409–422. <https://doi.org/10.1007/s10876-013-0620-1>
  27. Sichani GN, Morshed M, Amirnasr M, Abedi D (2009) In situ preparation, electrospinning, and characterization of polyacrylonitrile nanofibers containing silver nanoparticles. *J Appl Polym Sci* 116:1021–1029. <https://doi.org/10.1002/app.31436>
  28. Robert B, Nallathambi G (2021) Highly oriented poly (m-phenylene isophthalamide)/ polyacrylonitrile based coaxial nanofibers integrated with electrospun polyacrylonitrile-silver nanoparticle: application in air filtration of particulate and microbial contaminants. *J App Polym Sci*. <https://doi.org/10.1002/app.52294>



29. He M, Chen M, Dou Y, Ding J, Yue H, Yin G, Chen X, Cui Y (2020) Electrospun silver nanoparticles-embedded feather keratin/poly(vinyl alcohol)/poly(ethylene oxide) antibacterial composite nanofibers. *Polym* 12:305. <https://doi.org/10.3390/polym12020305>
30. Lu WC, Chen CY, Cho CJ, Venkatesan M, Chiang WH, Yu YY, Lee CH, Lee RH, Rwei SP, Kuo CC (2021) Antibacterial activity and protection efficiency of polyvinyl butyral nanofibrous membrane containing thymol prepared through vertical electrospinning. *Polymer* 13:1122. <https://doi.org/10.3390/polym13071122>
31. Zhu M, Hua D, Pan H, Wang F, Manshian B, Soenen SJ, Xiong R, Huang C (2018) Green electrospun and crosslinked poly(vinyl alcohol)/poly(acrylic acid) composite membranes for antibacterial effective air filtration. *J Colloid Interface Sci* 511:411–423. <https://doi.org/10.1016/j.jcis.2017.09.101>
32. Jiji S, Thenmozhi S, Kadirvelu K (2018) Comparison on properties and efficiency of bacterial and electrospun cellulose nanofibers. *Fibers Polym* 19:2498–2506. <https://doi.org/10.1016/j.apsusc.2019.07.020>
33. Chen KN, Sari FNI, Ting JM (2019) Multifunctional TiO<sub>2</sub>/polyacrylonitrile nanofibers for high efficiency PM2.5 capture, UV filter, and anti-bacteria activity. *Appl Surf Sci* 493:157–164. <https://doi.org/10.1016/j.apsusc.2019.07.020>
34. Shen B, Zhang D, Wei Y, Zhao Z, Ma X, Zhao X, Wang S, Yang W (2019) Preparation of Ag doped keratin/PA6 nanofiber membrane with enhanced air filtration and antimicrobial properties. *Polymer* 11:1511. <https://doi.org/10.3390/polym11091511>
35. Bortolassi AC, Nagarajan S, de Araújo LB, Guerra VG, Aguiar ML, Huon V, Soussan L, Cornu D, Miele P, Bechelany M (2019) Efficient nanoparticles removal and bactericidal action of electrospun nanofibers membranes for air filtration. *Mater Sci Eng C* 102:718–729. <https://doi.org/10.1016/j.msec.2019.04.094>
36. Canalli Bortolassi AC, Guerra VG, Aguiar ML, Soussan L, Cornu D, Miele P, Bechelany M (2019) Composites based on nanoparticle and pan electrospun nanofiber membranes for air filtration and bacterial removal. *Nanomate* 9(12):1740. <https://doi.org/10.3390/nano9121740>
37. Zhang L, Li L, Wang L, Nie J, Ma G (2020) Multilayer electrospun nanofibrous membranes with antibacterial property for air filtration. *Appl Surf Sci* 515:145962. <https://doi.org/10.1016/j.apsusc.2020.145962>
38. Patil NA, Gore PM, Prakash NJ, Govindaraj P, Yadav R, Verma V, Shanmugarajan D, Patil S, Kore A, Kandasubramanian B (2021) Needleless electrospun phytochemicals encapsulated nanofiber based 3-ply biodegradable mask for combating COVID-19 pandemic. *Chem Eng J* 416:129152. <https://doi.org/10.1016/j.cej.2021.129152>
39. Saikaew R, Intasanta V (2021) Versatile nanofibrous filters against fine particulates and bioaerosols containing tuberculosis and virus: Multifunctions and scalable processing. *Sep Purif Technol* 275:119171. <https://doi.org/10.1016/j.seppur.2021.119171>
40. Zhu Z, Zhang Y, Bao L, Chen J, Duan S, Chen SC, Xu P, Wang WN (2021) Self-decontaminating nanofibrous filters for efficient particulate matter removal and airborne bacteria inactivation. *Environ Sci Nano* 8:1081. <https://doi.org/10.1039/d0en01230k>
41. Blosi M, Costa AL, Ortelli S, Belosi F, Ravegnani F, Varesano A, Tonetti C, Zanoni I, Vineis C (2021) Polyvinyl alcohol/silver electrospun nanofibers: Biocidal filter media capturing virus size particles. *J Appl Polym Sci* 138(46):51380. <https://doi.org/10.1002/app.51380>

**Publisher's Note** Springer Nature remains neutral with regard to jurisdictional claims in published maps and institutional affiliations.

Springer Nature or its licensor (e.g. a society or other partner) holds exclusive rights to this article under a publishing agreement with the author(s) or other rightsholder(s); author self-archiving of the accepted manuscript version of this article is solely governed by the terms of such publishing agreement and applicable law.